Journal of Computational Mathematics
Vol.xx, No.x, 2023, 1–25.

http://www.global-sci.org/jcm
doi:10.4208/jcm.2308-m2023-0029

A CELL-CENTERED MULTIGRID SOLVER FOR THE FINITE VOLUME DISCRETIZATION OF ANISOTROPIC ELLIPTIC INTERFACE PROBLEMS ON IRREGULAR DOMAINS*

Kejia Pan
School of Mathematics and Statistics, HNP-LAMA, Central South University, Changsha 410083, China
Email: kejiapan@csu.edu.cn
Xiaoxin Wu[1)]
School of Mathematics and Statistics, HNP-LAMA, Central South University, Changsha 410083, China
Email: wuxiaoxin@csu.edu.cn
Hongling Hu
Key Laboratory of Computing and Stochastic Mathematics (Ministry of Education), School of Mathematics and Statistics, Hunan Normal University, Changsha 410081, China
Email: honglinghu@hunnu.edu.cn
Zhilin Li
Department of Mathematics, North Carolina State University, Raleigh, NC 27695-8205, USA
Email: zhilin@math.ncsu.edu

Abstract

The aim of this paper is to develop a fast multigrid solver for interpolation-free finite volume (FV) discretization of anisotropic elliptic interface problems on general bounded domains that can be described as a union of blocks. We assume that the curved interface falls exactly on the boundaries of blocks. The transfinite interpolation technique is applied to generate block-wise distorted quadrilateral meshes, which can resolve the interface with fine geometric details. By an extensive study of the harmonic average point method, an interpolation-free nine-point FV scheme is then derived on such multi-block grids for anisotropic elliptic interface problems with non-homogeneous jump conditions. Moreover, for the resulting linear algebraic systems from cell-centered FV discretization, a high-order prolongation operator based fast cascadic multigrid solver is developed and shown to be robust with respect to both the problem size and the jump of the diffusion coefficients. Various non-trivial examples including four interface problems and an elliptic problem in complex domain without interface, all with tens of millions of unknowns, are provided to show that the proposed multigrid solver is dozens of times faster than the classical algebraic multigrid method as implemented in the code AMG1R5 by Stüben.

Mathematics subject classification: 65N08, 65N55.
Key words: Elliptic interface problem, Discontinuous coefficients, Anisotropic coefficients, Cascadic multigrid method, Richardson extrapolation.

1. Introduction

In this paper we consider the following anisotropic elliptic interface problem:

* Received February 9, 2023 / Revised version received June 1, 2023 / Accepted August 9, 2023 / Published online December 13, 2023 /
1) Corresponding author

$$-\nabla \cdot (\kappa \nabla u) = f \quad \text{in } \Omega^+ \cup \Omega^-, \tag{1.1}$$
$$u = u_D \quad \text{on } \partial\Omega, \tag{1.2}$$
$$[u] = v \quad \text{on } \Gamma, \tag{1.3}$$
$$[\kappa \nabla u \cdot \mathbf{n}] = w \quad \text{on } \Gamma \tag{1.4}$$

on a bounded domain $\Omega = \Omega^+ \cup \Gamma \cup \Omega^- \in \mathbb{R}^2$. The subdomains Ω^+ and Ω^- are separated by the interface $\Gamma = \Omega^+ \cap \Omega^-$. The diffusion coefficient κ is a 2×2 symmetric positive definite matrix whose eigenvalues satisfy $\lambda_i \geq \lambda_0 > 0, i = 1, 2$, κ^+ and κ^- are restrictions of κ on Ω^+ and Ω^-, respectively, that is,

$$\kappa = \begin{pmatrix} \kappa_{11} & \kappa_{12} \\ \kappa_{12} & \kappa_{22} \end{pmatrix} = \begin{cases} \kappa^+, & \in \Omega^+, \\ \kappa^-, & \in \Omega^-, \end{cases}$$

in which κ may be discontinuous across the interface and causes a low global regularity of u, $f \in C(\Omega \setminus \Gamma)$ is a source term. The two jump conditions

$$v = u^+ - u^-, \quad w = \kappa^+ \nabla u^+ \cdot \mathbf{n} - \kappa^- \nabla u^- \cdot \mathbf{n}$$

are known functions across the interface Γ with at least C^1 continuity, and $\mathbf{n}$ is the unit normal direction pointing to the outer boundary (see Fig. 1.1). When $v = w = 0$ and the diffusion coefficient is continuous ($\kappa^+ = \kappa^-$), the problem degenerates into an anisotropic elliptic boundary value problem.

This type of problems occurs widely in the modeling of many physical phenomena such as crystal growths, Hele-Shaw flows, etc. Mathematically, it usually leads to partial differential equations with discontinuous or non-smooth solutions across interfaces. Hence, classical numerical methods designed for smooth solutions do not work efficiently. And many new methods have been developed in the last four decades, which can be roughly classified into two categories by using either an unfitted mesh (e.g. a uniform Cartesian mesh) or an interface-fitted (also known as body-fitted or interface conforming) mesh in the discretization of the domain.

In the unfitted mesh approach, the numerical approximation methods are modified locally near the interface to satisfy the jump conditions, of which two typical ones are the immersed interface method [31] and immersed finite element method [32]. The most attractive feature of the unfitted mesh approach is the easiness of the mesh generation, which is convenient for moving interface problems. Recent progress on the unfitted mesh approach can be found in [16, 18].

In this work, we focus on the interface-fitted mesh approach, which can be divided into three types: completely unstructured grid, locally unstructured grid, and semi-structured grid.

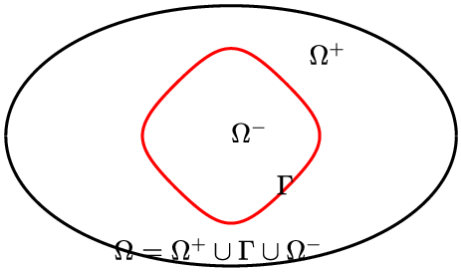

Fig. 1.1. An illustration of a general bounded domain with a curved interface.

The completely unstructured mesh generator is time consuming as it needs to modify the mesh for the whole domain, not just near the interface. The locally unstructured mesh generator [9] modifies just the mesh near the interface thus is more efficient than that of a completely unstructured grid. However, this local modification may damage the mesh quality near the interface and cause problems for fast solvers. In this paper, we are interested in the semi-structured and interface-fitted mesh approach, which can be regarded as a grid formed by splicing several blocks of structured grids with interface falling exactly on the boundaries of certain blocks.

The emphasis of this paper is to develop an efficient multigrid (MG) solver for the large scale anisotropic elliptic interface problems with strong discontinuity defined across the interface. There are at least three main challenges for such problems:

- The linear system of equations with millions of unknowns makes it impossible to use the direct solvers that need huge memories and unacceptable long time computations.
- The strong discontinuity in diffusion coefficients often leads to ill-conditioned system of linear equations for which iterative solvers would take too long to converge.
- Irregular geometries lead to either irregular grids or irregular discretizing points, which would worsen thecondition of the linear system and reduce the robustness of MG methods.

These challenges preclude standard MG methods, and many MG methods have been developed for addressing those challenges.

For elliptic interface problems with homogeneous jump conditions, Alcouffe *et al.* [4] proposed the first vertex-centered MG method for strongly discontinuous coefficients in 1981, in which diffusion coefficients are used in the design of interpolation operators. Wesseling *et al.* [48] developed the first cell-centered MG method by designing constant prolongation and restriction operators. Then Khalil *et al.* [28] gave a comparison between vertex-centered and cell-centered MG methods, which showed that the former were more robust and needed fewer iterations when convergent but the latter used less storage because of the constant transfer operators. In 1999, V-cycle MG method for two-dimensional elliptic equations with discontinuous constant coefficients was proposed by Kwak [30], in which new prolongation operators with energy bound were presented. In 2000, interface preserving coarsening algorithms were presented for complex interface problems by Wan *et al.* [46], thus only an easy linear interpolation operator was needed. Also in 2000, MG on the interface for mortar mixed finite element methods for elliptic problems was developed by Wheeler *et al.* [49], which reduced the algebraic system to a positive definite interface problem in the mortar spaces and then solved the problem using an MG algorithm on the interface with conjugate gradient smoothing. In 2001, an MG algorithm was presented for the mortar element method for the P1 nonconforming element by Xu *et al.* [52], in which the optimality of W-cycle MG was proved and a variable V-cycle MG pre-conditioner was constructed. In 2002, a cascadic multigrid (CMG) method for elliptic problems with strong material jumps is proposed and analyzed by Braess *et al.* [7], in which non-matching grids at interfaces between the sub-domains are allowed and treated by mortar elements. In 2008, uniform convergent MG methods for linear finite element (FE) approximation of second-order elliptic boundary value problems with strongly discontinuous coefficients were proposed by Xu [51]. In 2012, cell-centered MG methods for elliptic problems on semi-structured triangular grids with constant coefficients and discontinuous coefficients were proposed by Salinas [41, 42] and then further investigated for local Fourier analysis in [40]. In 2015, some two-level mortar domain

decomposition preconditioners for heterogeneous elliptic problems were investigated in [5]. In 2019, a local Fourier analysis for cell-centered MG method with discontinuous coefficients was proposed by Kumar *et al.* [29]. Also in 2019, geometric MG algorithms for the immersed finite element methods for elliptic problems with the interface were developed by Jo *et al.* [26], in which the transfer operators between levels were carefully defined. And this work was further developed for the semi-uniform grid [27] by introducing uniform grids as the auxiliary spaces. In 2020, based on a novel prolongation operator for the unfitted finite element space and an interface smoother, an MG method with more robustness for large jumps in the diffusion coefficients was developed. In 2021, a robust MG method for the 1D immersed finite element method (IFEM) was developed by Wang *et al.* [47], in which a rigorous theoretical analysis for the MG method based on the IFEM was given.

For elliptic interface problems with nonhomogeneous jump conditions, new geometric MG methods were developed by Adams *et al.* [3] for the maximum principle preserving immersed interface method in 2002, which was improved in [1] by giving a new interpolator for grid points near the immersed interface and a new restrictor that guarantees the coarse-grid matrices are M-matrices. And a comparison of these two methods with algebraic MG was presented in [2]. In 2003, an algebraic MG solver was applied to the three-dimensional interface problems by Deng *et al.* [15]. In 2006, a standard MG solver was applied to solve the linear problem resulting from FV method for the solution of the two-dimensional elliptic equation by Oevermann *et al.* [35], and an algebraic MG was applied to the three-dimensional case [36]. In 2007, the algebraic MG method was employed for a coupling interface method under the Cartesian grid for solving elliptic complex interface problems in arbitrary dimensions by Chern *et al.* [11]. In 2008, a Krylov-accelerated interface MG approach was proposed for the piecewise-polynomial interface method for elliptic problems with complex interfaces between high-contrast materials by Chen *et al.* [10]. In 2012, an easy-to-implement MG method led by new Lagrange multiplier spaces that achieve near-optimal efficiency was proposed by Hellrung *et al.* [22], which can achieve near-optimal efficiency for irregular domains. Also in 2012, an MG approach with a suitable definition of the restriction operator is provided for the one-dimensional second-order accurate Ghost Fluid Method by Coco *et al.* [12], and extensions to 2D and 3D cases were given in [14]. Once again in 2012, a quasi-algebraic MG approach to fracture problems based on extended finite elements was proposed by Hiriyur *et al.* [23]. In 2014, the bilinear and linear immersed finite element solutions generated from the algebraic MG solver for both stationary and moving interface problems were discussed by Feng *et al.* [19]. In 2020, an optimal MG solver for arbitrary order extended finite element methods based on two discontinuous Galerkin schemes were studied by Xiao *et al.* [50]. In 2021, an optimal MG algorithm for combining P1-Q1 finite element approximations of interface problems based on local anisotropic fitting meshes was proposed by Hu *et al.* [25].

Cascadic multigrid (CMG) method proposed by Deuflhard and Bornemann [6] is a variant of the MG without any coarse grid correction step, where instead of starting from the finest grid, the solution is first computed on the coarsest grid and the recursively interpolated and relaxed on finer grids (see Fig. 1.2). Based on a new Richardson extrapolation formula for the linear FE solution, an extrapolation cascadic multigrid (EXCMG) method was first proposed by Chen *et al.* [8] to solve the 2D Poisson equation with the linear FE discretization. For the EXCMG method, to obtain a better initial guess of the iterative solution on the next finer grid, numerical solutions on the two-level of grids (current and previous grids) are needed (whereas only one-level of the numerical solution is needed in the CMG method). The EX-

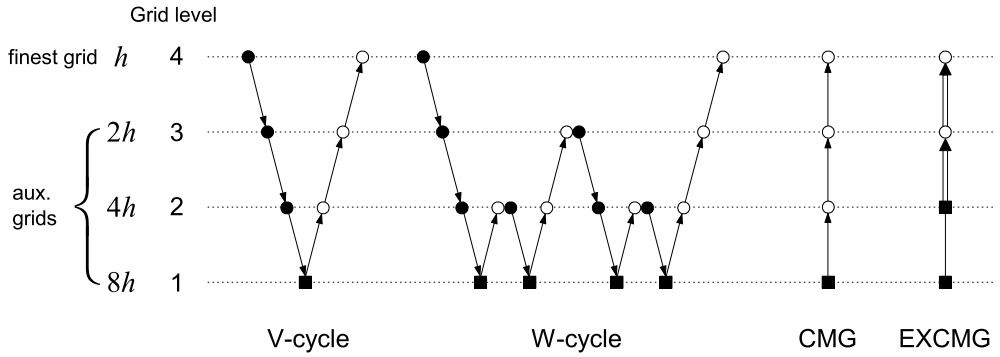

Fig. 1.2. Four kinds of multigrid methods [37].

CMG algorithm has been successfully applied to smooth problems with finite difference (FD) and FE discretization in two- and three-dimension [24, 37, 38]. However, as far as we know, the EXCMG algorithm has mainly been used for solving the linear system resulting from the vertex-centered FD or FE discretization of two- and three-dimensional smooth problems. It is of more importance to solve general cell-centered FV schemes for elliptic interface problems.

In this paper, we develop a new EXCMG method combined with a cell-centered finite volume (FV) scheme for solving two-dimensional anisotropic elliptic interface problems with strongly discontinuous coefficients and nonhomogeneous jump conditions defined along an interface. Firstly, the irregular geometry of the interface is overcome by separating the domain into quadrilateral blocks with edges aligned with the interface. And the transfinite interpolation (TFI) method first proposed by Gordon *et al.* [17, 20, 21] is applied to generate structured body-fitting quadrilateral grids, which receives its name due to how a function belonging to this class is able to match the primitive function at a nondenumerable number of points. Then, for the discontinuity across the interface, we generalize the homogenization function proposed by Terekhov *et al.* [45] to the nonhomogeneous case and derive a cell-centered interpolation-free FV discretization for elliptic interface problems. Finally, for the large scale linear system resulting from cell-centered FV discretization, we design a new constant block-wise prolongation operator by the Lagrangian interpolation and extend the EXCMG algorithm to non-nested and semi-structured grids and non-smooth problems.

The rest of the paper is organized as follows. Section 2 gives a brief review of the mesh generation algorithm based on the TFI method and the description of the FV discretization for the anisotropic elliptic interface problems. In Section 3, we present the prolongation operator and EXCMG algorithm in detail. Section 4 contains the numerical results to demonstrate the high efficiency and accuracy of the proposed method. And conclusions are given in the final section.

2. Body-Fitting Quadrilateral Mesh Generator

In this section, we introduce the interface-fitted mesh generator based on the transfinite interpolation method. We first describe the algorithm for a single quadrilateral block and then give a unified mesh generation algorithm. In addition, one oblique interface example is presented to illustrate the algorithm.

2.1. Transfinite interpolation in a single quadrilateral block

Interpolation generally refers to a given finite number of points and finding the curve passing through these points. The interpolation object of transfinite interpolation is a curve, that is, infinite points, which is also the source of the word "transfinite". Transfinite interpolation generates grids by performing interpolation using boundary curves [17, 21].

Let $\mathcal{B}(\xi,\eta)$ be a curved quadrilateral domain where the grid needs to be generated, and $\mathcal{B}_L(\eta)=\mathcal{B}(0,\eta),\mathcal{B}_R(\eta)=\mathcal{B}(1,\eta),\mathcal{B}_D(\xi)=\mathcal{B}(\xi,0)$ and $\mathcal{B}_U(\xi)=\mathcal{B}(\xi,1)$ be the four boundaries of $\mathcal{B}$, in which $(\xi,\eta)\in[0,1]\times[0,1]$ (See Fig. 2.1). Then $\mathcal{B}(\xi,\eta)$ can be expressed by boundaries based on the following formula:

$$\begin{aligned}\mathcal{B}(\xi,\eta)=&(1-\xi)\mathcal{B}_L(\eta)+\xi\mathcal{B}_R(\eta)+(1-\eta)\mathcal{B}_D(\xi)+\eta\mathcal{B}_U(\xi)-\xi\eta\mathcal{B}_U(1)\\&-(1-\xi)\eta\mathcal{B}_U(0)-(1-\eta)\xi\mathcal{B}_D(1)-(1-\xi)(1-\eta)\mathcal{B}_D(0).\end{aligned}\tag{2.1}$$

Finally, an algorithm for mesh generation on single curved quadrilateral domain is given in Algorithm 2.1.

Algorithm 2.1: Mesh Generation Algorithm for Single Curved Quadrilateral Domain.

Step 1. Determine the numbers N_ξ and N_η of grid nodes in two coordinate directions.

Step 2. Obtain all boundary nodes

$$\mathcal{B}_L\left(\frac{i}{N_\eta}\right),\quad \mathcal{B}_R\left(\frac{i}{N_\eta}\right),\quad \mathcal{B}_D\left(\frac{j}{N_\xi}\right),\quad \mathcal{B}_U\left(\frac{j}{N_\xi}\right),\quad i=1,\ldots,N_\eta,\quad j=1,\ldots,N_\xi.$$

Step 3. Obtain by (2.1) all mesh nodes

$$\mathcal{B}\left(\frac{j}{N_\xi},\frac{i}{N_\eta}\right),\quad i=1,\ldots N_\eta,\quad j=1,\ldots N_\xi.$$

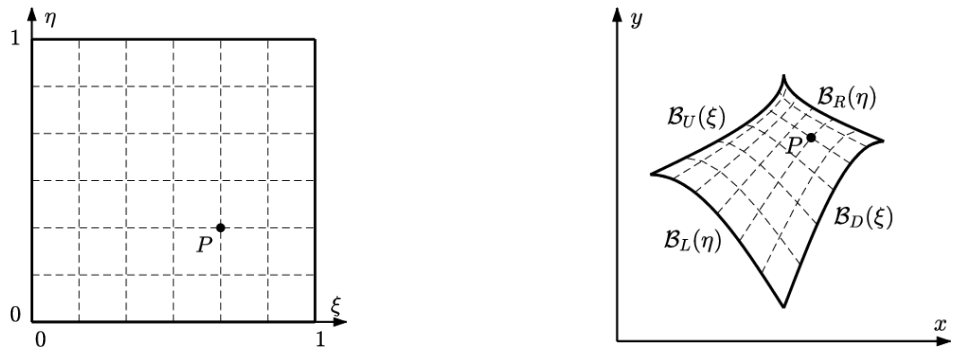

(a) Logical domain (b) Physical domain

Fig. 2.1. Illustration of TFI projection.

2.2. A unified mesh generation algorithm

For the application to irregular geometry of the interface, we need the following assumption.

Assumption 2.1. *The solution domain can be divided into several non-overlapping curved quadrilateral subdomains naturally conformal with the material interface.*

Remark 2.1. Assumption 2.1 may not be satisfied for the extremely irregular geometries, but it is suitable for general cases since the edge can be curved which makes it quite flexible.

With this assumption, irregular geometries of boundary and interface can be easily conquered by simply applying mesh generation algorithm to each curved quadrilateral subdomains. A unified mesh generation algorithm for complex domain with curved interface and boundary is given in Algorithm 2.2. An example for mesh generation of a rectangle domain with oblique interface is given in Fig. 2.2.

Algorithm 2.2: Mesh Generation Algorithm for Complex Domain with Curved Interface and Boundary.
Step 1. Decompose the domain into several non-overlapping curved quadrilateral subdomains naturally conformal with the problem boundary and interface. Step 2. Generate structured body-fitting quadrilateral mesh for each subdomain by using Algorithm 2.1.

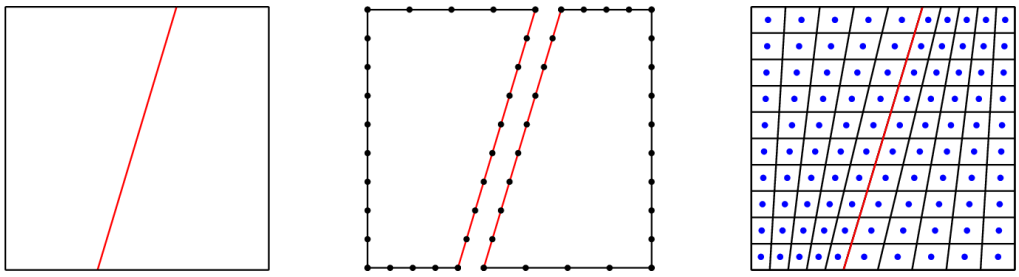

(a) Oblique interface (b) Divided (c) Block mesh

Fig. 2.2. Illustration of mesh generation process.

3. Interpolation-Free FV Schemes for Elliptic Interface Problems

3.1. Preliminaries

According to Algorithm 2.2, the interface Γ is always located on the edges of mesh cells, which means that there is no mixed material cell. For each inner cell that has no intersection point with the boundary, there are four common-faced cells. And by introducing edge centers on the boundary as stencil points for cells having intersection points with boundary, five stencil points are available for all cells (See Fig. 3.1).

We denote the cell and the cell center by K and L, the vertex by A and B, and cell edge by σ. If σ is a common edge of cells K and L, and its vertices are A and B, then we denote

$$\sigma = K|L = BA.$$

Let $K_{A,\sigma}$ be the adjacent cell of K that intersects with edge σ on only one point A. And let $K_{B,\sigma}$ be the adjacent cell of K that intersects with edge σ on only one point B (see Fig. 3.2).

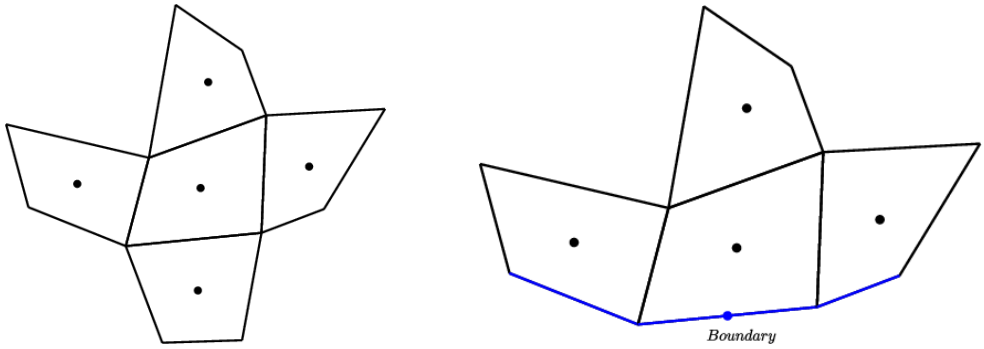

(a) Inner cell (b) Boundary cell

Fig. 3.1. Five-point stencil for cell-centered discretization.

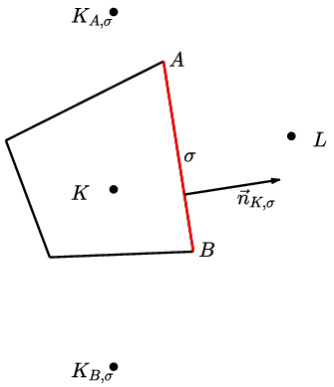

Fig. 3.2. Some notations for stencil.

Let $\mathcal{J}$ be the set of all cells, ε the set of all cell-edges, ε_{int} the set of all cell-edges not on $\partial\Omega$, ε_{ext} the set of all cell-edges on $\partial\Omega$, and ε_K the set of all edges of cell K. Denote $h = \sup_{K\in\mathcal{J}} d(K)$, where $d(K)$ is the diameter of cell K.

By integrating the Eq. (1.1) over cell K and using Green formula, we obtain

$$\sum_{\sigma\in\varepsilon_K} \mathcal{F}_{K,\sigma} = \int_K f(\mathbf{x})d\mathbf{x}, \tag{3.1}$$

where $\mathcal{F}_{K,\sigma}$ is the continuous normal flux through σ, defined by

$$\mathcal{F}_{K,\sigma} = -\int_\sigma \kappa(\mathbf{x})\nabla u(\mathbf{x})\cdot\vec{n}(\mathbf{x})dl = -\int_\sigma \nabla u(\mathbf{x})\cdot\kappa_K^T\vec{n}_{K,\sigma}dl \tag{3.2}$$

with $\vec{n}_{K,\sigma}$ being the unit outward normal vector on the edge σ of cell K (see Fig. 3.3). Next we consider how to discretize the continuous flux numerically.

3.2. Handling discontinuities using a homogenization technique

Firstly, we propose a homogenization technique to deal with the discontinuity on the material interface. The idea of homogenization was first proposed by Terekhov *et al.* in [45] to deal with the diffusion problem, which can be used to approximate directional derivatives in heterogeneous

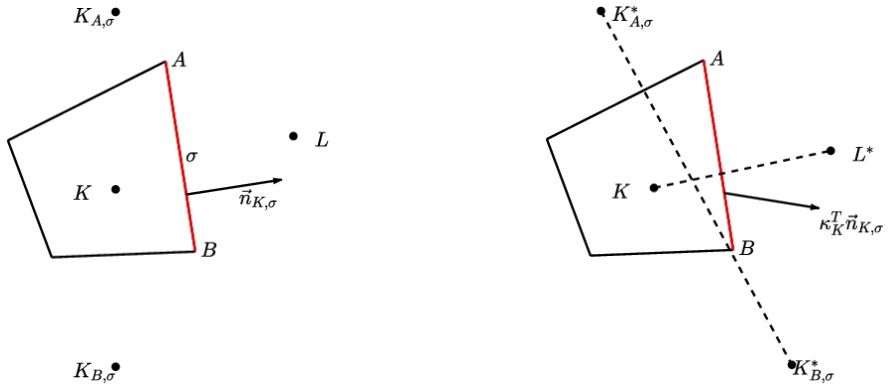

(a) Before homogenization (b) After homogenization

Fig. 3.3. Some notations for edge σ.

media. In this paper, we extend it to the elliptic interface problem with non-homogenous jumping conditions using a much simpler deduction.

Assume that gradients of u are constant in each cell. By the jump conditions (1.3)-(1.4), we have

$$\nabla u_K \cdot \vec{t}_\sigma = \nabla u_L \cdot \vec{t}_\sigma + \delta_{K,L}, \tag{3.3}$$

$$\kappa_K \nabla u_K \cdot \vec{n}_{K,\sigma} + \kappa_L \nabla u_L \cdot \vec{n}_{L,\sigma} = \xi_\sigma, \tag{3.4}$$

where κ_K and κ_L are values of κ on σ from cells K and L, respectively, $\vec{t}_\sigma$ is the unit tangent vector on the edge σ,

$$\delta_{K,L} = \begin{cases} 0, & \sigma \notin \Gamma, \\ \nabla v_\sigma \cdot \vec{t}_\sigma, & K \in \Omega^+, \quad L \in \Omega^-, \\ -\nabla v_\sigma \cdot \vec{t}_\sigma, & K \in \Omega^-, \quad L \in \Omega^+, \end{cases}$$

$$\xi_\sigma = \begin{cases} 0, & \sigma \notin \Gamma, \\ -w_\sigma, & K \in \Omega^+, \quad L \in \Omega^-, \\ w_\sigma, & K \in \Omega^-, \quad L \in \Omega^+, \end{cases}$$

∇v_σ and w_σ are the average value of $\nabla v(\mathbf{x})$ and $w(\mathbf{x})$ on σ, respectively. Rewriting (3.3) and (3.4) into matrix form, we can obtain

$$\nabla u_L = T_{L,K} \nabla u_K + C_{L,K}, \tag{3.5}$$

where

$$T_{L,K} = \left(\left[\vec{t}_\sigma, -\kappa_L^T \vec{n}_{L,\sigma} \right]^T \right)^{-1} \left(\left[\vec{t}_\sigma, \kappa_K^T \vec{n}_{K,\sigma} \right]^T \right)$$

is called as homogenization matrix, and

$$C_{L,K} = - \left(\left[\vec{t}_\sigma, -\kappa_L^T \vec{n}_{L,\sigma} \right]^T \right)^{-1} \left[\delta_{K,L}, \xi_\sigma \right]^T$$

is called as homogenization constant vector.

Secondly, we will show how to distort the space geometry to overcome the discontinuity caused by interface based on the homogenization technique. Denote the edge center of σ as I, $u(I)|_K = \lim_{\mathbf{x}\to I,\mathbf{x}\in K} u(\mathbf{x})$ and $u(I)|_L = \lim_{\mathbf{x}\to I,\mathbf{x}\in L} u(\mathbf{x})$ be the limit value of $u(I)$ from cells K and L, respectively.

Based on multivariate Taylor expansion, we have

$$\begin{aligned} u(L) &= u(L) - u(I)|_L + u(I)|_L - u(I)|_K + u(I)|_K - u(K) + u(K) \\ &= \nabla u_L \cdot \overrightarrow{IL} + \eta_{K,L} + \nabla u_K \cdot \overrightarrow{KI} + u(K) \\ &= (T_{L,K}\nabla u_K + C_{L,K}) \cdot \overrightarrow{IL} + \eta_{K,L} + \nabla u_K \cdot \overrightarrow{KI} + u(K) \\ &= \nabla u_K \cdot \big(\overrightarrow{KI} + T_{L,K}^T \overrightarrow{IL}\big) + \big(\eta_{K,L} + C_{L,K} \cdot \overrightarrow{IL}\big) + u(K), \end{aligned} \tag{3.6}$$

where

$$\eta_{K,L} = \begin{cases} 0, & \sigma \notin \Gamma, \\ -v(I), & K \in \Omega^+, \quad L \in \Omega^-, \\ v(I), & K \in \Omega^-, \quad L \in \Omega^+. \end{cases}$$

Denote $L^* = K + (\overrightarrow{KI} + T_{L,K}^T \overrightarrow{IL})$ and $C_{K,L}^* = (\eta_{K,L} + C_{L,K} \cdot \overrightarrow{IL})$, we can obtain

$$u(L) = u(K) + \nabla u_K \cdot \overrightarrow{KL^*} + C_{K,L}^*. \tag{3.7}$$

Similarly, we have

$$u(K_{A,\sigma}) = u(K) + \nabla u_K \cdot \overrightarrow{KK_{A,\sigma}^*} + C_{K,K_{A,\sigma}}^*, \tag{3.8}$$

$$u(K_{B,\sigma}) = u(K) + \nabla u_K \cdot \overrightarrow{KK_{B,\sigma}^*} + C_{K,K_{B,\sigma}}^*, \tag{3.9}$$

where $K_{A,\sigma}^*, K_{B,\sigma}^*, C_{K,K_{A,\sigma}}^*$ and $C_{K,K_{B,\sigma}}^*$ have similar definitions as L^* and $C_{K,L}^*$, respectively.

3.3. Discretization of continuous fluxes

Finally, we consider the discretization of continuous flux. Decomposing the co-normal vector $\kappa_K^T \vec{n}_{K,\sigma}$ into two directions $\overrightarrow{K_{A,\sigma}^* K_{B,\sigma}^*}$ and $\overrightarrow{KL^*}$, we have

$$\kappa_K^T \vec{n}_{K,\sigma} = \alpha_{K,\sigma} \overrightarrow{KL^*} + \beta_{K,\sigma} \overrightarrow{K_{A,\sigma}^* K_{B,\sigma}^*}, \tag{3.10}$$

where

$$\alpha_{K,\sigma} = \frac{\big(\kappa_K^T \vec{n}_{K,\sigma}, M_R \overrightarrow{K_{A,\sigma}^* K_{B,\sigma}^*}\big)}{\big(\overrightarrow{KL^*}, M_R \overrightarrow{K_{A,\sigma}^* K_{B,\sigma}^*}\big)}, \quad \beta_{K,\sigma} = \frac{\big(\kappa_K^T \vec{n}_{K,\sigma}, M_R \overrightarrow{KL^*}\big)}{\big(\overrightarrow{K_{A,\sigma}^* K_{B,\sigma}^*}, M_R \overrightarrow{KL^*}\big)},$$

and

$$M_R = \begin{pmatrix} 0 & -1 \\ 1 & 0 \end{pmatrix}$$

is rotation matrix. Substituting (3.10) into (3.2) and using (3.7)-(3.9), we can obtain

$$\begin{aligned} \mathcal{F}_{K,\sigma} &= -\int_\sigma \nabla u(\mathbf{x}) \cdot \kappa_K^T \vec{n}_{K,\sigma} dl \\ &= -\int_\sigma \nabla u(\mathbf{x}) \cdot \Big(\alpha_{K,\sigma} \overrightarrow{KL^*} + \beta_{K,\sigma} \overrightarrow{K_{A,\sigma}^* K_{B,\sigma}^*}\Big) dl \end{aligned}$$

$$
\begin{aligned}
&= -\int_{\sigma} \nabla u(\mathbf{x}) \cdot \left(\alpha_{K,\sigma}\overrightarrow{KL^*} + \beta_{K,\sigma}\overrightarrow{KK^*_{B,\sigma}} - \beta_{K,\sigma}\overrightarrow{KK^*_{A,\sigma}}\right) dl \\
&= \alpha_{K,\sigma}\big(u(K) - u(L)\big) + \beta_{K,\sigma}\big(u(K_{A,\sigma}) - u(K_{B,\sigma})\big) \\
&\quad + \alpha_{K,\sigma}C^*_{K,L} + \beta_{K,\sigma}\big(C^*_{K,K_{B,\sigma}} - C^*_{K,K_{A,\sigma}}\big) + \mathcal{O}(h^2). \qquad (3.11)
\end{aligned}
$$

Similarly, we can obtain

$$
\begin{aligned}
\mathcal{F}_{L,\sigma} &= \alpha_{L,\sigma}\big(u(L) - u(K)\big) + \beta_{L,\sigma}\big(u(L_{B,\sigma}) - u(L_{A,\sigma})\big) \\
&\quad + \alpha_{L,\sigma}C^*_{L,K} + \beta_{L,\sigma}\big(C^*_{L,L_{A,\sigma}} - C^*_{L,L_{B,\sigma}}\big) + \mathcal{O}(h^2). \qquad (3.12)
\end{aligned}
$$

To obtain a conservative discretization for continuous flux, we integrate (3.4) on σ and obtain

$$
\mathcal{F}_{K,\sigma} = -\int_{\sigma} \xi_{\sigma} dl - \mathcal{F}_{L,\sigma}. \qquad (3.13)
$$

The conservative continuous flux $\bar{\mathcal{F}}_{K,\sigma}$ can be obtained by a linear combination of two one-side fluxes as

$$
\bar{\mathcal{F}}_{K,\sigma} = \mu_1 \mathcal{F}_{K,\sigma} + \mu_2 \left(-\int_{\sigma} \xi_{\sigma} dl - \mathcal{F}_{L,\sigma}\right), \qquad (3.14)
$$

where $\mu_1 = \alpha_{L,\sigma}/(\alpha_{K,\sigma} + \alpha_{L,\sigma})$ and $\mu_2 = 1 - \mu_1$. And the conservative continuous flux $\bar{\mathcal{F}}_{K,\sigma}$ can be written as

$$
\begin{aligned}
\bar{\mathcal{F}}_{K,\sigma} &= \frac{2\alpha_{K,\sigma}\alpha_{L,\sigma}}{\alpha_{K,\sigma} + \alpha_{L,\sigma}}\big(u(K) - u(L)\big) + \frac{\alpha_{L,\sigma}\beta_{K,\sigma}}{\alpha_{K,\sigma} + \alpha_{L,\sigma}}\big(u(K_{A,\sigma}) - u(K_{B,\sigma})\big) \\
&\quad + \frac{\alpha_{K,\sigma}\beta_{L,\sigma}}{\alpha_{K,\sigma} + \alpha_{L,\sigma}}\big(u(L_{A,\sigma}) - u(L_{B,\sigma})\big) + \bar{C}_{K,\sigma} + \mathcal{O}(h^2), \qquad (3.15)
\end{aligned}
$$

where

$$
\begin{aligned}
\bar{C}_{K,\sigma} &= \frac{\alpha_{K,\sigma}\alpha_{L,\sigma}}{\alpha_{K,\sigma} + \alpha_{L,\sigma}}\big(C^*_{K,L} - C^*_{L,K}\big) + \frac{\alpha_{L,\sigma}\beta_{K,\sigma}}{\alpha_{K,\sigma} + \alpha_{L,\sigma}}\big(C^*_{K,K_{B,\sigma}} - C^*_{K,K_{A,\sigma}}\big) \\
&\quad + \frac{\alpha_{K,\sigma}\beta_{L,\sigma}}{\alpha_{K,\sigma} + \alpha_{L,\sigma}}\big(C^*_{L,L_{B,\sigma}} - C^*_{L,L_{A,\sigma}}\big) - \frac{\alpha_{K,\sigma}\displaystyle\int_{\sigma} \xi_{\sigma} dl}{\alpha_{K,\sigma} + \alpha_{L,\sigma}}.
\end{aligned}
$$

By neglecting the high-order error, we get the following conservative discrete flux $F_{K,\sigma}$:

1) for $\sigma \in \varepsilon_{int}$,

$$
\begin{aligned}
F_{K,\sigma} &= \frac{2\alpha_{K,\sigma}\alpha_{L,\sigma}}{\alpha_{K,\sigma} + \alpha_{L,\sigma}}(u_K - u_L) + \frac{\alpha_{L,\sigma}\beta_{K,\sigma}}{\alpha_{K,\sigma} + \alpha_{L,\sigma}}(u_{K_{A,\sigma}} - u_{K_{B,\sigma}}) \\
&\quad + \frac{\alpha_{K,\sigma}\beta_{L,\sigma}}{\alpha_{K,\sigma} + \alpha_{L,\sigma}}(u_{L_{A,\sigma}} - u_{L_{B,\sigma}}) + \bar{C}_{K,\sigma}, \qquad (3.16)
\end{aligned}
$$

2) for $\sigma \in \varepsilon_{ext}$,

$$
\begin{aligned}
F_{K,\sigma} &= \alpha_{K,\sigma}(u_K - u_L) + \beta_{K,\sigma}(u_{K_{A,\sigma}} - u_{K_{B,\sigma}}) \\
&\quad + \alpha_{K,\sigma}C^*_{K,L} + \beta_{K,\sigma}\big(C^*_{K,K_{B,\sigma}} - C^*_{K,K_{A,\sigma}}\big). \qquad (3.17)
\end{aligned}
$$

Remark 3.1. For the conservative discrete flux, the nonhomogeneous jump conditions are embedded in the constants $\bar{C}_{K,\sigma}$ and $\alpha_{K,\sigma}C^*_{K,L} + \beta_{K,\sigma}(C^*_{K,K_{B,\sigma}} - C^*_{K,K_{A,\sigma}})$, thus only the right hand side of the linear system resulting from the FV discretization should be modified. This practice was first proposed in [34] but limited in constant diffusion coefficients and only with first-order accuracy.

3.4. The interpolation-free FV scheme

The FV scheme of the elliptic interface problem (1.1) is defined as follows:

$$\sum_{\sigma\in\varepsilon_K} F_{K,\sigma} = m(K)f_K, \quad K \in \mathcal{J}, \tag{3.18}$$

$$u_K = g_K, \qquad K \in \varepsilon_{ext}, \tag{3.19}$$

where $m(K)$ is the area of cell K, $f_K = f(K)$ and $g_K = g(K)$.

Remark 3.2. The cell-centered FV scheme proposed in this section does not introduce auxiliary unknowns defined on vertices or edge-centers which usually need to be approximated by some interpolation schemes. The new FV scheme is free of these interpolation works and the fixed nine-point stencil makes it efficient and easy to implement.

This scheme often leads to a nonsymmetric nine-diagonal coefficient matrix for general quadrilateral meshes. Only when the mesh line are orthogonal and the diffusion coefficients are constant, does the scheme reduce to the standard five-point scheme. And the discontinuity makes the linear system of low efficiency especially when the scale of the problem is large. Thus, it is of great importance to developing fast solvers for these problems such as multigrid methods, which will be described in the following section.

4. The Cell-Centered Extrapolation Cascadic Multigrid Method

In this section, we first discuss some problems caused by the irregularity of geometries and discontinuity across the interface and construct a new multigrid prolongation operator, then propose a CEXCMG method for solving the large-scale linear system of equations arising from interpolation-free FV discretizations of anisotropic elliptic interface problems with homogeneous jump conditions. This work can be regarded as an extension of our previous work on the CEXCMG method for solving the large linear system resulting from FV discretizations on the regular hexahedral mesh of diffusion equations with interfaces that are parallel to the axis [39].

4.1. Some challenges and solutions

The difficulties for designing multigrid method with the occurrence of curved interface for anisotropic elliptic interface problems can be summarized as the following three aspects:

- Curved boundary and interface prevent us from adopting structured regular meshes, which brings troubles for designing geometric multigrid methods.
- The nonhomogeneous jump conditions lead to the discontinuity of solutions across the interface.
- The strongly discontinuous diffusion coefficients make the resulting linear system extremely ill-conditioned and very difficult to solve.

For the first problem, our solution is to design a new multigrid prolongation operator on the logical domain by using the TFI method. Thus only some suitable interpolation algorithms for nested Cartesian grids are needed for consideration. For the second problem, our solution is to design a fully blocked prolongation operator by increasing the number of interpolation

points, and requires that the coarsest grids of each block have enough degrees of freedom. For the third problem, our solution is to develop an effective extrapolation technique to construct a high-order approximation to the FV solution on the next finer grid, which greatly reduces the number of required iterations of smoothing.

4.2. A fully blocked prolongation operator

Suppose that the FV solution u_h obtained from the Eqs. (3.18)-(3.19) has an asymptotic error expansion as follows:

$$u_h = u + \mathcal{S}(\mathbf{x})h^2 + \mathcal{O}(h^3), \tag{4.1}$$

where $S(\mathbf{x})$ is a block-wise smooth function independent of mesh size h. As discussed in the previous subsection, the FV solution is defined on the distorted grids in order to fit the interface and boundary. However, the interpolation on the distorted mesh will lead to the costly local linear system to solve. To overcome this problem, we reverse the TFI projection (see Fig. 4.1) and consider the interpolation on the logical domain (ξ, η). Then for each subdomain, we have

$$u_h\big(\mathbf{x}(\xi,\eta)\big) = u\big(\mathbf{x}(\xi,\eta)\big) + \mathcal{S}\big(\mathbf{x}(\xi,\eta)\big)h^2 + \mathcal{O}(h^3), \quad (\xi,\eta) \in [0,1]\times[0,1],$$

where $\mathcal{S}(\mathbf{x}(\xi,\eta))$ is a smooth function independent of mesh size h.

To make the prolongation operator with at least third-order accuracy and fully blocked, which means no interaction is involved between every two block, we take an interpolation element consisting of 3×3 neighboring coarse cells into account, and consider how to obtain values at 6×6 cell centers on the refined grid by interpolating the 3×3 numerical solutions on coarse cell (see Fig. 4.2). In Lagrange's form, the bi-quadratic interpolation polynomial is given by

$$w_h\big(\mathbf{x}(\xi,\eta)\big) = \sum_{i=1}^{3}\sum_{j=1}^{3} N_{i,j}\big(\mathbf{x}(\xi,\eta)\big)u_{2h}\left(\mathbf{x}\left(\frac{i-0.5}{3},\frac{j-0.5}{3}\right)\right) \doteq P_{2h}^{h}(u_{2h}), \tag{4.2}$$

$$\xi,\eta = \frac{l}{12}, \quad l = 1,3,5,\ldots,11,$$

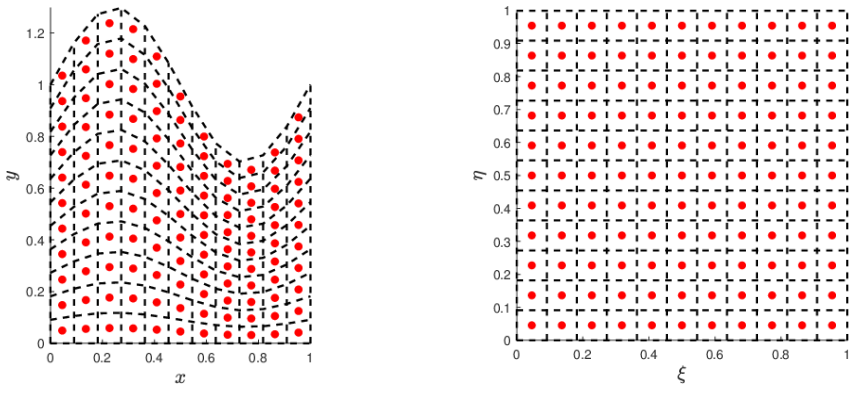

(a) Physical domain (b) Logical domain

Fig. 4.1. Illustration of reversed TFI projection.

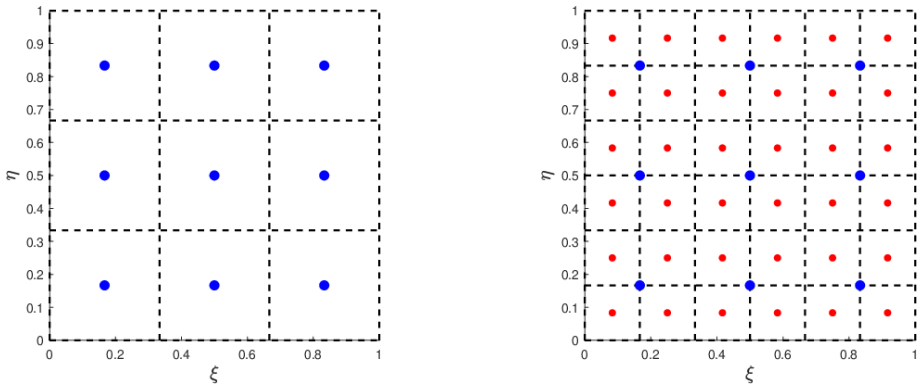

(a) Coarse mesh (b) Refined mesh

Fig. 4.2. Illustration of an interpolation element in logical domain.

where the Lagrange interpolation basis function $N_{i,j}$ is defined as follows [33]:

$$N_{i,j}\big(\mathbf{x}(\xi,\eta)\big)=\prod_{1\le k\le 3,\ k\neq i}\frac{\xi-(k-0.5)/3}{(i-0.5)/3-(k-0.5)/3}\prod_{1\le k\le 3,\ k\neq j}\frac{\eta-(k-0.5)/3}{(j-0.5)/3-(k-0.5)/3}. \tag{4.3}$$

Remark 4.1. The fully blocked prolongation operator defined in this subsection uses the bi-quadratic interpolation on each block. Thus the prolongation operator only introduces interpolation error of $\mathcal{O}(h^3)$. And we only need to handle the second-order term $S(\mathbf{x})h^2$ in the asymptotic error expansion, which can be eliminated by using an extrapolation technique in the following subsection.

4.3. The CEXCMG algorithm

In this subsection, we will state the whole procedure of the construction of high-order approximation to the FV solution U_h, and propose a CEXCMG algorithm for solving the elliptic interface problem with discontinuous and anisotropic coefficients.

For cell-centered FV solutions u_{4h} and u_{2h} obtained from the Eqs. (3.18)-(3.19), the prolongation operator $P_{2h,h}$ is applied as

$$u_{4h,h}=P_{2h,h}\big(P_{4h,2h}(u_{4h})\big),\quad u_{2h,h}=P_{2h,h}(u_{2h}).$$

Then the high-order approximation is obtained by extrapolation as

$$u_h^0=u_{2h,h}+\frac{1}{4}(u_{2h,h}-u_{4h,h}).$$

Finally, a new CEXCMG algorithm is obtained in Algorithm 4.1.

Remark 4.2. Usually, the number of each level of grids is set as follows:

$$m_k=m_L\cdot\beta^{L-k},\quad k=2,3,\ldots,L,$$

where m_L is the number of iterations on the finest grid, $\beta<2^d$ (d is the dimension of the computational domain). In such case, it is easy to show that the multigrid complexity of the CEXCMG method can be obtained.

Algorithm 4.1: Cell-Centered EXCMG.

Solve $A_0 u_0 = f_0$.
Solve $A_1 u_1 = f_1$.
for $k = 2$ *to* L **do**
  $u_k^0 := P_{k-1}^k(u_{k-1}) + \frac{1}{4}\big(P_{k-1}^k(u_{k-1}) - P_{k-1}^k\big(P_{k-2}^{k-1}(u_{k-2})\big)\big)$.
  Compute u_k by applying m_k smoothing steps to u_k^0

$$u_k := \mathrm{SMOOTH}^{m_k}\big(u_k^0, A_k, f_k\big).$$

end

Remark 4.3. In Algorithm 4.1, we take the BiCGStab iteration as the multigrid smoother instead of the conjugate gradient iteration used in the usual cascadic multigird method [6]. The BiCGStab is more suitable for nonsymmetric linear system resulting from the FV scheme (3.18)-(3.19).

5. Numerical Experiments

In this section, we will illustrate the efficiency of CEXCMG with the BiCGStab smoother by comparing with the classical algebraic multigrid (AMG) method as implemented in the code AMG1R5 by Stüben [44], and present numerical results obtained by these algorithms for five test examples, which contain two problems with irregular geometry, two problems with orders of magnitude discontinuity, and one problem on a complex domain without interface. Our code is written in Fortran 90 and compiled with Intel Visual Fortran Compiler XE 12.1 compiler. All programs are carried out on a server with Intel(R) Xeon(R) Gold 6248R CPU (3.0 GHz) and 192 GB RAM.

The order of convergence of the method is computed by

$$\mathrm{order} = \log_2 \frac{\| u_h - u \|}{\| u_{h/2} - u \|}, \tag{5.1}$$

where $\| \cdot \|$ denotes some norm (for instance, L^2-norm or L^∞-norm) and u is the exact solution. In all of tests the source term and boundary condition are determined by the true solution. For all tests we take $\epsilon = 10^{-12}$.

5.1. An oblique interface test

In this test, the computational domain Ω is set as $[-1, 1]^2$ which is separated into two sub-domains $\Omega^- = \{x \in \Omega : y < 2x\}$ and $\Omega^+ = \{x \in \Omega : y > 2x\}$ by an oblique interface $\Gamma = \{y = 2x \,|\, (x, y) \in \Omega\}$ passing through the domain center $(0, 0)$.

We designate the solution as

$$u(x, y) = \begin{cases} x^2 - y^2, & (x, y) \in \Omega^-, \\ \sin(x)\cos(y), & (x, y) \in \Omega^+, \end{cases}$$

and the anisotropic coefficient of the PDE is set as

$$\kappa^+ = \begin{pmatrix} 4 & 2 \\ 2 & 5 \end{pmatrix}, \quad \kappa^- = 10^5 \kappa^+.$$

The mesh generated by TFI is illustrated in Fig. 5.1.

The number of iterations on each level of grids is set to be $m_k = m_L \cdot 4^{L-k}$ with m_L being taken according to the accuracy requirement (10^{-10}). Table 5.1 shows the number of iterations on each level of grid, the error $\|u_h - u\|$, and the difference between the numerical solution and initial guess $\|u_h - u_h^0\|$. From the table, we can see that the numerical solution obtained by CEXCMG achieves second-order accuracy in the maximum norm with only 6 iterations on the finest grid; the difference between the numerical solution and the initial guess $||u_h - u_h^0||$ is 4.39×10^{-11} on the finest grid, and the initial guesses are of third-order accuracy. These fully illustrate the effectiveness of the CEXCMG method.

The CPU time of the CEXCMG and AMG1R5 solver are plotted in Fig. 5.2. We can see that the CEXCMG method is more than twenty times faster than the AMG1R5 method for solving the discrete problem with 26214400 degrees of freedom.

Table 5.1: Numerical results obtained by CEXCMG with BiCGStab smoother for oblique interface test. The total solving time is only 17.93 seconds.

No. of DoFs	Iter	$\|u_h - u\|_\infty$	Order	$\|u_h - u_h^0\|_2$	Order
25600	198	1.00e-4	1.92	2.12e-6	2.93
102400	375	2.61e-5	1.95	2.71e-7	2.97
409600	384	6.69e-6	1.96	3.43e-8	2.98
1638400	96	1.70e-6	1.98	3.17e-9	3.43
6553600	24	4.29e-7	1.99	3.57e-10	3.15
26214400	6	1.07e-7	2.00	4.39e-11	3.02

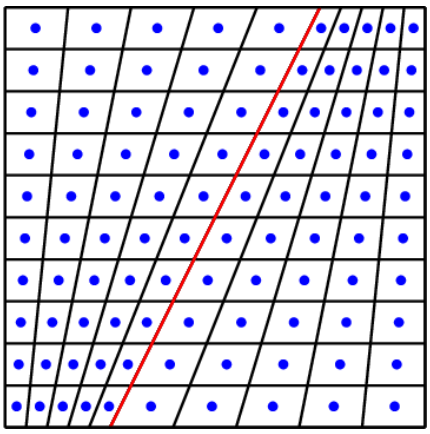

Fig. 5.1. Illustration of mesh with oblique interface.

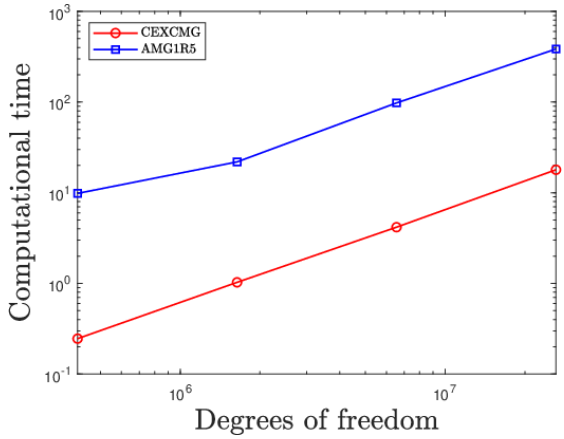

Fig. 5.2. Comparison of computational times of CEXCMG and AMG1R5 for oblique interface test.

5.2. A curved interface test

In this test, the computational domain Ω is set as $[-1,1]^2$ which is separated into two subdomains $\Omega^- = \{(x,y) \in \Omega : 0.1\sin(pi * y) < x\}$ and $\Omega^+ = \{(x,y) \in \Omega : 0.1\sin(pi * y) > x\}$ by curved interface $\Gamma = \{x = 0.1\sin(pi * y) | (x,y) \in \Omega\}$.

We designate the solution as

$$u(x,y) = \begin{cases} e^x \cos(y), & (x,y) \in \Omega^-, \\ x^2 + y^2, & (x,y) \in \Omega^+, \end{cases}$$

and the anisotropic coefficient of the PDE is set as a piecewise variable function

$$\kappa^+ = \begin{pmatrix} x^2+y^2+1 & x^2+y^2 \\ x^2+y^2 & x^2+y^2+2 \end{pmatrix}, \quad \kappa^- = 10^5 \kappa^+.$$

The mesh generated by TFI is illustrated in Fig. 5.3.

The challenge of the example is that the interface is curved. The results in Table 5.2 agree with our analysis. Fig. 5.4 shows that the CEXCMG method is more than one hundred times faster than the AMG1R5 method for solving the discrete problem with 26214400 degrees of freedom.

Table 5.2: Numerical results obtained by CEXCMG with BiCGStab smoother for curved interface test. The total solving time is only 46.49 seconds.

No. of DoFs	Iter	$\|u_h - u\|_\infty$	Order	$\|u_h - u_h^0\|_2$	Order
25600	185	9.31e-5	1.97	2.08e-6	2.97
102400	283	2.35e-5	1.98	2.82e-7	2.89
409600	461	5.92e-6	1.99	3.79e-8	2.90
1638400	144	1.48e-6	2.00	4.11e-9	3.20
6553600	36	3.71e-7	2.00	2.24e-10	4.19
26214400	9	9.29e-8	2.00	2.13e-11	3.40

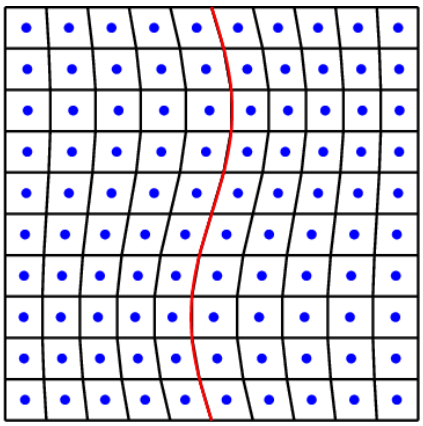

Fig. 5.3. Illustration of mesh with curved interface.

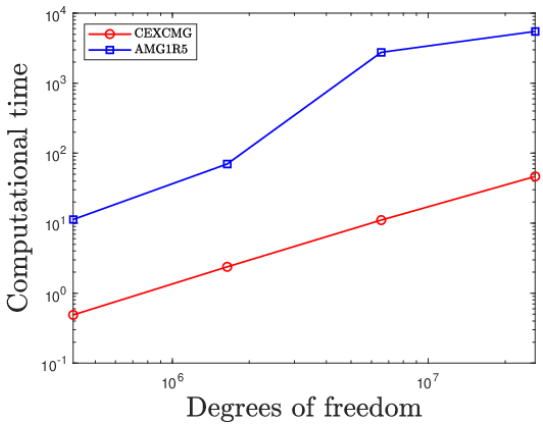

Fig. 5.4. Comparison of computational times of CEXCMG and AMG1R5 for curved interface test.

5.3. A circle interface test with a strong discontinuity

In this test, the computational domain Ω is set as $[-1,1]^2$ which is separated into two subdomains $\Omega^- = \{(x,y) \in \Omega : x^2+y^2 < 0.6^2\}$ and $\Omega^+ = \{(x,y) \in \Omega : x^2+y^2 > 0.6^2\}$ by a circle interface $\Gamma = \{x^2+y^2 = 0.6^2 | (x,y) \in \Omega\}$.

We designate the solution as

$$u(x,y) = \begin{cases} \sin(x+y), & (x,y) \in \Omega^-, \\ e^{x+y}, & (x,y) \in \Omega^+, \end{cases}$$

and the anisotropic coefficient of the PDE is set as

$$\kappa^+ = 10^{10} \begin{pmatrix} 1 & -0.5 \\ -0.5 & 1 \end{pmatrix}, \quad \kappa^- = \begin{pmatrix} 1 & 0.5 \\ 0.5 & 1 \end{pmatrix}.$$

The mesh generated by TFI is illustrated in Fig. 5.5.

The challenges of the example are that the interface is a circle, the mesh is multi-blocked and the diffusion coefficient is of orders of magnitude discontinuity. The results in Table 5.3

agree with our analysis. Fig. 5.6 shows that the CEXCMG method is more than two hundred times faster than the AMG1R5 method for solving the discrete problem with 19660800 degrees of freedom.

Table 5.3: Numerical results obtained by CEXCMG with BiCGStab smoother for strong discontinuity test with circle interface. The total solving time is only 34.86 seconds.

No. of DoFs	Iter	$\|u_h - u\|_\infty$	Order	$\|u_h - u_h^0\|_2$	Order
19200	578	8.51e-5	1.97	8.12e-6	2.38
76800	1255	2.15e-5	1.99	1.28e-6	2.66
307200	576	5.40e-6	1.99	1.81e-7	2.83
1228800	144	1.35e-6	2.00	2.11e-8	3.10
4915200	36	3.33e-7	2.02	2.31e-9	3.19
19660800	9	8.11e-8	2.04	2.75e-10	3.08

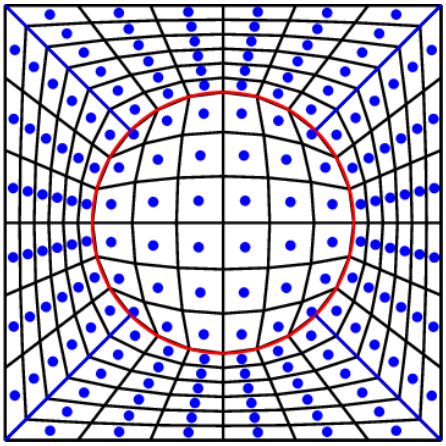

Fig. 5.5. Illustration of mesh with circle interface.

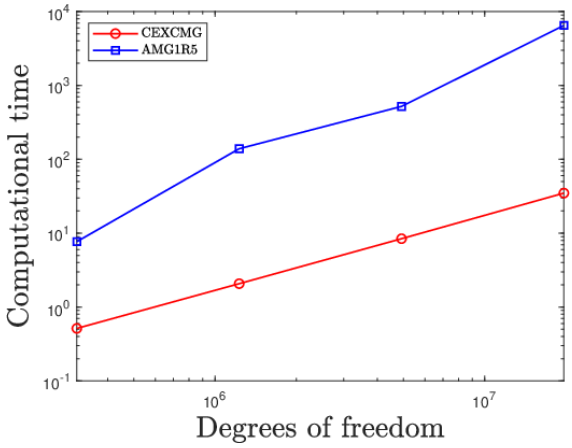

Fig. 5.6. Comparison of computational times of CEXCMG and AMG1R5 for circle interface test.

5.4. A rectangular interface test with a strong discontinuity

In this test, the computational domain Ω is set as an ellipse $\{(x,y)|x^2+4y^2<5^2\}$ which is separated into two sub-domains $\Omega^- = \{(x,y)\in\Omega : |x|<1,\ |y|<1\}$ and $\Omega^+ = \{(x,y)\in\Omega : |x|>1,\ \text{or}\ |y|>1\}$.

We designate the solution as

$$u(x,y) = \begin{cases} \cos(x)+y, & (x,y)\in\Omega^-, \\ \sin(xy), & (x,y)\in\Omega^+, \end{cases}$$

and the anisotropic coefficient of the PDE is set as

$$\kappa^+ = 10^5 \begin{pmatrix} 1 & -0.5 \\ -0.5 & 1 \end{pmatrix}, \quad \kappa^- = 10^{-5} \begin{pmatrix} 1 & 0.5 \\ 0.5 & 1 \end{pmatrix}.$$

The mesh generated by TFI is illustrated in Fig. 5.7.

The challenges of the example are that the interface is a rectangular, the domain is an ellipse and the diffusion coefficient is of orders of magnitude discontinuity. The results in Table 5.4 agree with our analysis. From Table 5.5, we can conclude that the runtimes of the mesh generation part can be ignored compared with the assembling and solving parts. Fig. 5.8 shows that the CEXCMG method is more than two hundred times faster than the AMG1R5 method for solving the discrete problem with 28311552 degrees of freedom.

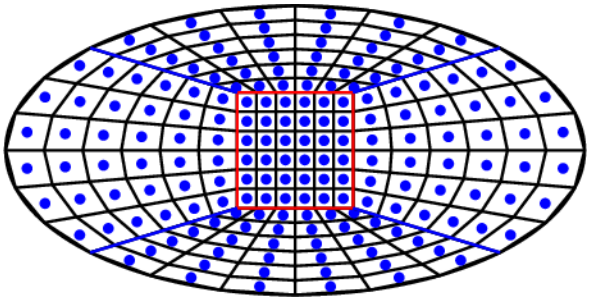

Fig. 5.7. Illustration of mesh with rectangular interface.

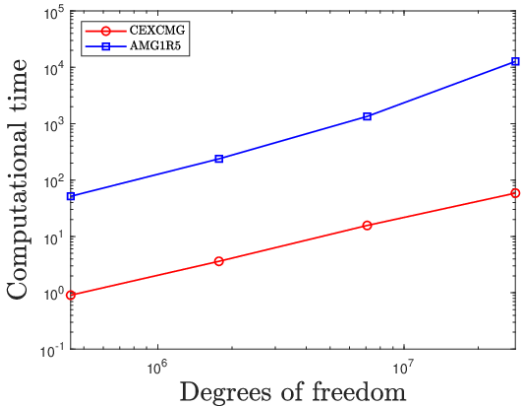

Fig. 5.8. Comparison of computational times of CEXCMG and AMG1R5 for rectangular interface test.

Table 5.4: Numerical results obtained by CEXCMG with BiCGStab smoother for strong discontinuity test with rectangular interface. The total solving time is only 58.60 seconds.

No. of DoFs	Iter	$\|u_h - u\|_\infty$	Order	$\|u_h - u_h^0\|_2$	Order
27648	299	5.54e-3	1.99	1.58e-3	3.11
110592	511	1.38e-3	2.00	2.11e-4	2.90
442368	576	3.47e-4	2.00	2.64e-5	3.00
1769472	144	8.68e-5	2.00	3.26e-6	3.02
7077888	36	2.17e-5	2.00	4.03e-7	3.02
28311552	9	5.42e-6	2.00	5.03e-8	3.00

Table 5.5: CPU time (in seconds) for strong discontinuity test with rectangular interface.

No. of DoFs	Assemble	Solve	Mesh
442368	0.5696	0.90	0.0348
1769472	2.3046	3.61	0.1494
7077888	9.8401	15.63	0.5753
28311552	39.1361	58.60	3.0918

5.5. A non-smooth domain test with highly anisotropic coefficients

In this test, the computational domain $\Omega = \Omega_1 \cup \Omega_2$ is taken according to [13], where Ω_1 is a circle centered at $(-0.25, 0)$ and radius 0.55, and Ω_2 is a circle centered at $(0.25, 0)$ and the same radius 0.55 (See Fig. 5.9).

We designate the solution as

$$u(x, y) = \sin(x) + y,$$

and the diffusion coefficient of the PDE is set as

$$\kappa^+ = \kappa^- = \begin{pmatrix} 10^8 & 0 \\ 0 & 1 \end{pmatrix}.$$

The mesh generated by TFI is illustrated in Fig. 5.9.

The challenge of the example is that the the domain is a union of two circles. The results in Table 5.6 agree with our analysis. Fig. 5.10 shows that the CEXCMG method is more than eighty times faster than the AMG1R5 method for solving the discrete problem with 26214400 degrees of freedom.

Table 5.6: Numerical results obtained by CEXCMG with BiCGStab smoother for general domain test without interface. The total solving time is only 41.36 seconds.

No. of DoFs	Iter	$\|u_h - u\|_\infty$	Order	$\|u_h - u_h^0\|_2$	Order
25600	193	3.24e-5	1.99	1.00e-6	3.44
102400	344	8.13e-6	2.00	1.95e-7	2.36
409600	564	2.03e-6	2.00	3.90e-8	2.33
1638400	144	5.08e-7	2.00	7.46e-9	2.39
6553600	36	1.27e-7	2.00	4.65e-10	4.00
26214400	9	3.18e-8	2.00	3.99e-11	3.54

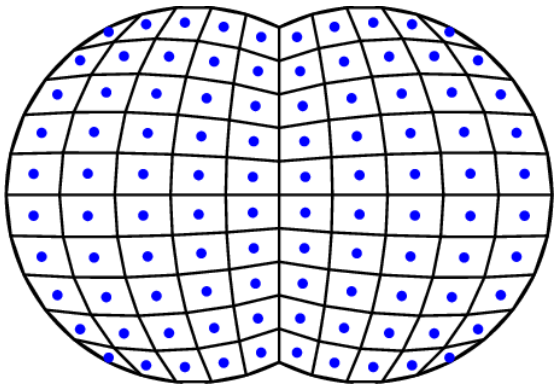

Fig. 5.9. Illustration of mesh on general domain.

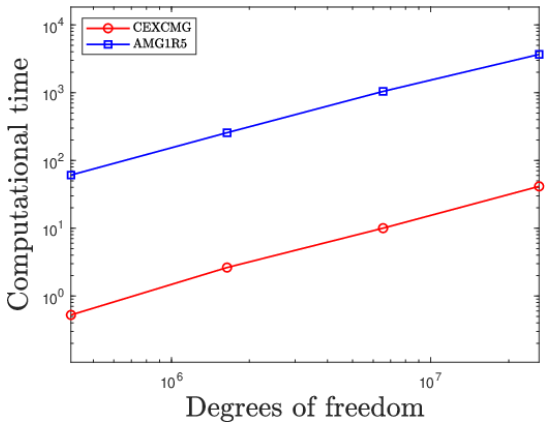

Fig. 5.10. Comparison of computational times of CEXCMG and AMG1R5 for general domain test without interface.

6. Conclusions

In this paper, we develop a new EXCMG method combined with a cell-centered FV scheme for solving two-dimensional anisotropic elliptic interface problems with strongly discontinuous coefficients and nonhomogeneous jump conditions defined along an interface. Firstly, the irregular geometries of the interface are overcome by separating the domain into quadrilateral blocks with curved edges aligned with the interface. And transfinite interpolation method proposed by Gordon *et al.* [21] is applied to generate structured body-fitting quadrilateral grids. Then, for the discontinuity across the interface, we generalize the homogenization function proposed by Terekhov [45] to nonhomogeneous cases and derive a cell-centered FV discretization for elliptic interface problems. Finally, for the large scale linear system resulting from cell-centered FV discretization, we design a new constant block-wise prolongation operator by the Lagrangian interpolation and extend the EXCMG algorithm to non-nested grids and non-smooth problems. Our method can obviously solve elliptic boundary value problems in complex domains [13, 43].

Acknowledgements. We would like to thank the Editor and two anonymous reviewers for their valuable suggestions and careful reading which have helped us to improve the paper.

K.J. Pan was supported by the National Natural Science Foundation of China (Grant No. 42274101). X.X. Wu was supported by the Fundamental Research Funds for the Central Universities of Central South University (Grant No. 2020zzts354). H.L. Hu was supported by the National Natural Science Foundation of China (Grant No. 12071128) and by the Natural Science Foundation of Hunan Province (Grant No. 2021JJ30434). Z.L. Li was supported by a Simons Grant No. 633724.

References

[1] L. Adams and T.P. Chartier, New geometric immersed interface multigrid solvers, *SIAM J. Sci. Comput.*, **25**:5 (2004), 1516–1533.

[2] L. Adams and T. Chartier, A comparison of algebraic multigrid and geometric immersed interface multigrid methods for interface problems, *SIAM J. Sci. Comput.*, **26**:3 (2005), 762–784.

[3] L. Adams and Z. Li, The immersed interface/multigrid methods for interface problems, *SIAM J. Sci. Comput.*, **24**:2 (2002), 463–479.

[4] R.E. Alcouffe, A. Brandt, J.E. Dendy, and J.W. Painter, The multi-grid methods for the diffusion equation with strongly discontinuous coefficients, *SIAM J. Sci. Stat. Comput.*, **2**:4 (1981), 430–454.

[5] T. Arbogast and H. Xiao, Two-level mortar domain decomposition preconditioners for heterogeneous elliptic problems, *Comput. Methods Appl. Mech. Engrg.*, **292** (2015), 221–242.

[6] F.A. Bornemann and P. Deuflhard, The cascadic multigrid method for elliptic problems, *Numer. Math.*, **75** (1996), 135–152.

[7] D. Braess, P. Deuflhard, and K. Lipnikov, A subspace cascadic multigrid method for mortar elements, *Computing*, **69** (2002), 205–225.

[8] C. Chen, H. Hu, Z.Q. Xie, and C. Li, Analysis of extrapolation cascadic multigrid method (EXCMG), *Sci. China Ser. A-Math.*, **51**:8 (2008), 1349–1360.

[9] L. Chen, H. Wei, and M. Wen, An interface-fitted mesh generator and virtual element methods for elliptic interface problems, *J. Comput. Phys.*, **334** (2017), 327–348.

[10] T. Chen and J. Strain, Piecewise-polynomial discretization and Krylov-accelerated multigrid for elliptic interface problems, *J. Comput. Phys.*, **227**:16 (2008), 7503–7542.

[11] I. Chern and Y. Shu, A coupling interface method for elliptic interface problems, *J. Comput. Phys.*, **225**:2 (2007), 2138–2174.

[12] A. Coco and G. Russo, Second order multigrid methods for elliptic problems with discontinuous coefficients on an arbitrary interface, I: One dimensional problems, *Numer. Math. Theory Methods Appl.*, **5**:1 (2012), 19–42.

[13] A. Coco and G. Russo, Finite-difference ghost-point multigrid methods on Cartesian grids for elliptic problems in arbitrary domains, *J. Comput. Phys.*, **241** (2013), 464–501.

[14] A. Coco and G. Russo, Second order finite-difference ghost-point multigrid methods for elliptic problems with discontinuous coefficients on an arbitrary interface, *J. Comput. Phys.*, **361** (2018), 299–330.

[15] S. Deng, K. Ito, and Z. Li, Three-dimensional elliptic solvers for interface problems and applications, *J. Comput. Phys.*, **184**:1 (2003), 215–243.

[16] B. Dong, X. Feng, and Z. Li, An FE-FD method for anisotropic elliptic interface problems, *SIAM J. Sci. Comput.*, **42**:4 (2020), B1041–B1066.

[17] C. Dyken and M.S. Floater, Transfinite mean value interpolation, *Comput. Aided Geom. Design*, **26**:1 (2009), 117–134.

[18] Q. Feng, B. Han, and P. Minev, A high order compact finite difference scheme for elliptic interface problems with discontinuous and high-contrast coefficients, *Appl. Math. Comput.*, **431** (2022), 127314.

[19] W. Feng, X. He, Y. Lin, and X. Zhang, Immersed finite element method for interface problems with algebraic multigrid solver, *Commun. Comput. Phys.*, **15**:4 (2014), 1045–1067.

[20] A. Garon and M. Delfour, Mesh adaptation based on transfinite mean value interpolation, *J. Comput. Phys.*, **407** (2020), 109248.
[21] W.J. Gordon and C.A. Hall, Transfinite element methods: Blending-function interpolation over arbitrary curved element domains, *Numer. Math.*, **21**:2 (1973), 109–129.
[22] J.L. Hellrung, L. Wang, E. Sifakis, and J.F. Teran, A second order virtual node method for elliptic problems with interfaces and irregular domains in three dimensions, *J. Comput. Phys.*, **231**:4 (2012), 2015–2048.
[23] B. Hiriyur, R. Tuminaro, H. Waisman, E. Boman, and D. Keyes, A quasi-algebraic multigrid approach to fracture problems based on extended finite elements, *SIAM J. Sci. Comput.*, **34**:2 (2012), A603–A626.
[24] H. Hu, Z. Ren, D. He, and K. Pan, On the convergence of an extrapolation cascadic multigrid method for elliptic problems, *Comput. Math. Appl.*, **74**:4 (2017), 759–771.
[25] J. Hu and H. Wang, An optimal multigrid algorithm for the combining P_1-Q_1 finite element approximations of interface problems based on local anisotropic fitting meshes, *J. Sci. Comput.*, **88**:1 (2021), 16.
[26] G. Jo and D.Y. Kwak, Geometric multigrid algorithms for elliptic interface problems using structured grids, *Numer. Algorithms*, **81**:1 (2019), 211–235.
[27] G. Jo and D. Kwak, A semi-uniform multigrid algorithm for solving elliptic interface problems, *Comput. Methods Appl. Math.*, **21**:1 (2021), 127–143.
[28] M. Khalil and P. Wesseling, Vertex-centered and cell-centered multigrid for interface problems, *J. Comput. Phys.*, **98**:1 (1992), 1–10.
[29] P. Kumar, C. Rodrigo, F.J. Gaspar, and C.W. Oosterlee, On local Fourier analysis of multigrid methods for PDEs with jumping and random coefficients, *SIAM J. Sci. Comput.*, **41**:3 (2019), A1385–A1413.
[30] D. Kwak, V-cycle multigrid for cell-centered finite differences, *SIAM J. Sci. Stat. Comput.*, **21**:2 (1999), 552–564.
[31] R.J. LeVeque and Z. Li, The immersed interface method for elliptic equations with discontinuous coefficients and singular sources, *SIAM J. Numer. Anal.*, **31**:4 (1994), 1019–1044.
[32] Z. Li, T. Lin, and X. Wu, New Cartesian grid methods for interface problems using the finite element formulation, *Numer. Math.*, **96**:1 (2003), 61–98.
[33] G. Liu, S. Quek, *The Finite Element Method: A Practical Course*, Butterworth-Heinemann, 2013.
[34] X. Liu, R.P. Fedkiw, and M. Kang, A boundary condition capturing method for Poisson's equation on irregular domains, *J. Comput. Phys.*, **160**:1 (2000), 151–178.
[35] M. Oevermann and R. Klein, A Cartesian grid finite volume method for elliptic equations with variable coefficients and embedded interfaces, *J. Comput. Phys.*, **219**:2 (2006), 749–769.
[36] M. Oevermann, C. Scharfenberg, and R. Klein, A sharp interface finite volume method for elliptic equations on Cartesian grids, *J. Comput. Phys.*, **228**:14 (2009), 5184–5206.
[37] K. Pan, D. He, and H. Hu, An extrapolation cascadic multigrid method combined with a fourth-order compact scheme for 3D Poisson equation, *J. Sci. Comput.*, **70**:3 (2017), 1180–1203.
[38] K. Pan, D. He, H. Hu, and Z. Ren, A new extrapolation cascadic multigrid method for three dimensional elliptic boundary value problems, *J. Comput. Phys.*, **344** (2017), 499–515.
[39] K. Pan, X. Wu, H. Hu, Y. Yu, and Z. Li, A new FV scheme and fast cell-centered multigrid solver for 3D anisotropic diffusion equations with discontinuous coefficients, *J. Comput. Phys.*, **449** (2022), 110794.
[40] C. Rodrigo, P. Salinas, F. Gaspar, and F. Lisbona, Local Fourier analysis for cell-centered multigrid methods on triangular grids, *J. Comput. Appl. Math.*, **259** (2014) 35–47.
[41] P. Salinas, C. Rodrigo, F. Gaspar, and F. Lisbona, Multigrid methods for cell-centered discretizations on triangular meshes, *Numer. Linear Algebra Appl.*, **20**:4 (2013), 626–644.
[42] P. Salinas, C. Rodrigo, F. Gaspar, and F. Lisbona, An efficient cell-centered multigrid method for problems with discontinuous coefficients on semi-structured triangular grids, *Comput. Math.*

Appl., **65**:12 (2013), 1978–1989.

[43] K.M. Singh and J.J.R. Williams, A parallel fictitious domain multigrid preconditioner for the solution of Poisson's equation in complex geometries, *Comput. Methods Appl. Mech. Engrg.*, **194**:45-47 (2005), 4845–4860.

[44] K. Stüben, Algebraic multigrid (AMG): Experiences and comparisons, *Appl. Math. Comput.*, **13**:3-4 (1983), 419–451.

[45] K.M. Terekhov, B.T. Mallison, and H.A. Tchelepi, Cell-centered nonlinear finite-volume methods for the heterogeneous anisotropic diffusion problem, *J. Comput. Phys.*, **330** (2017), 245–267.

[46] W.L. Wan, Interface preserving coarsening multigrid for elliptic problems with highly discontinuous coefficients, *Numer. Linear Algebra Appl.*, **7**:7-8 (2000), 727–741.

[47] S. Wang, F. Wang, and X. Xu, A robust multigrid method for one dimensional immersed finite element method, *Numer. Methods Partial Differ. Equ.*, **37**:3 (2021), 2244–2260.

[48] P. Wesseling, Cell centered multigrid for interface problems, *J. Comput. Phys.*, **79**:1 (1988), 85–91.

[49] M.F. Wheeler and I. Yotov, Multigrid on the interface for mortar mixed finite element methods for elliptic problems, *Comput. Methods Appl. Mech. Engrg.*, **184**:2-4 (2000), 287–302.

[50] Y. Xiao, J. Xu, and F. Wang, High-order extended finite element methods for solving interface problems, *Comput. Methods Appl. Mech. Engrg.*, **364** (2020), 112964.

[51] J. Xu and Y. Zhu, Uniform convergent multigrid methods for elliptic problems with strongly discontinuous coefficients, *Math. Models Methods Appl. Sci.*, **18**:1 (2008), 77–105.

[52] X. Xu and J. Chen, Multigrid for the mortar element method for P1 nonconforming element, *Numer. Math.*, **88** (2001), 381–398.